Optical Channel Capacity Sensitivity

J. Hamkins,[1] S. Dolinar,[1] and D. Divsalar[1]

A previous article [1] defined fundamental parameters that determine the capacity of pulse-position modulation (PPM) on a soft-decision optical channel under various statistical models. This article describes the relationship between the four fundamental parameters and a multitude of physical parameters that describe the laser, channel, and detector. Using this relationship and the gradient of capacity, the sensitivity of capacity with respect to each fundamental and physical parameter is derived. Numerical results indicate that, over a wide range of operating points, a single fundamental parameter dominates the capacity calculation. Capacity was found to be more sensitive to the signal intensity than to the background intensity—typically by a factor of approximately two—and the quantum efficiency of a detector was found to be the single most important detector parameter. Leakage currents have virtually no impact on the capacity.

I. Introduction

A previous article [1] defined four fundamental parameters, ρ_0, ρ_+, Δ, and β_0, that are sufficient to determine the capacity of M-pulse-position modulation (PPM) on a soft-decision optical channel. Loosely speaking, these parameters describe the slot signal-to-noise ratio (SNR), the "excess" SNR arising from different variances in signaling and nonsignaling slots, the "skewness" of the Webb distribution, and the closeness of the signal to the Gaussian distribution.

The Free-space Optical Communication Analysis Software (FOCAS)[2] used by NASA to determine optical link budgets uses 79 physical parameters, including: laser, relay optics, telescope, and pointing parameters of the transmitter; modulation and coding formats of the signal; noise sources and atmospheric parameters; and telescope, relay optics, detector, and amplifier parameters of the receiver. These physical parameters affect capacity through their effects on the four fundamental parameters. In order to evaluate

[1] Communications Systems and Research Section.

[2] M. Jeganathan and S. Mecherle, *A Technical Manual for FOCAS 2.0—Free-Space Optical Communications Analysis Software*, JPL unpublished internal document, Jet Propulsion Laboratory, Pasadena, California, May 1998.

The research described in this publication was carried out by the Jet Propulsion Laboratory, California Institute of Technology, under a contract with the National Aeronautics and Space Administration.

the sensitivity of capacity with respect to any given physical parameters, we explore more deeply the relationship between fundamental and physical parameters. For a full description of the physical parameters, see, e.g., [2,4].[3] The physical parameters we consider in this article are

(1) *Laser and Modulator Parameters.* Laser and modulator parameters include the optical frequency, ν; the width of the pulse slot, T_s; the required dead time between pulses, T_d; the modulation extinction ratio, α_{er}; and the order M of the M-ary PPM signal.

(2) *Detector Parameters.* Avalanche photodiode (APD) detector parameters include the quantum efficiency, η; excess noise factor, F; gain, G; noise temperature, T; load resistance, R_L; bulk leakage current, I_b; and surface leakage current, I_s.

(3) *Channel Parameters.* Channel parameters include the mean number of background photons incident on the detector, $\bar{n}_b$, and the mean number of pulse-induced photons incident on the detector, $\bar{n}_s$.

Some other parameters can be expressed in terms of those above but will not be used explicitly in this article. For example, the ionization ratio, k_{eff}, is related to F and G by $F = k_{eff}G + (2 - 1/G)(1 - k_{eff})$; the noise equivalent one-sided bandwidth, B, is set equal to $1/2T_s$; and the optical frequency, ν, only matters in how it affects $\bar{n}_b$ and $\bar{n}_s$. The dead time, T_d, has no bearing on capacity expressed in bits per channel use. However, T_d is very relevant for the total throughput, in bits per second. (The slot width, T_s, *is* relevant to the capacity expressed in bits per channel use, because the level of thermal noise per slot depends on T_s.) And for most lasers, α_{er} has a negligible effect, being on the order of 10^6. Hence, in the remainder of the article, ν, T_d, and α_{er} will be ignored.

II. Capacity of the Webb-Plus-Gaussian Channel

In [1], the capacity of the standard additive white Gaussian noise channel (AWGN-1), a more general AWGN channel (AWGN-2), a Webb-distributed channel (Webb-2), and a blended Webb and Gaussian channel (Webb+Gaussian) were considered. Here, we concentrate on the Webb+Gaussian channel, which models both the avalanche process in an APD and the thermal noise process in follow-on electronics.

A. Channel Model

Each slot statistic y_i at the output of an APD is a Webb+Gaussian distributed random variable [1]:

$$y_i \sim \begin{cases} W(m_1, \sigma_1^2, \delta_1^2) + N(m', \sigma'^2) & \text{signaling slot} \\ W(m_0, \sigma_0^2, \delta_0^2) + N(m', \sigma'^2) & \text{nonsignaling slot} \end{cases} \tag{1}$$

[3] Ibid.

where $W(m,\sigma^2,\delta^2) = m + \sigma W(0,1,\delta^2)$ is a shifted, scaled version of the zero-mean, unit-variance Webb random variable $W(0,1,\delta^2)$ that has probability density

$$\phi(w;\delta^2) \triangleq \frac{1}{\sqrt{2\pi}} \left(\frac{1+w}{\delta}\right)^{-3/2} e^{-w^2/2(1+w/\delta)}, \quad w > -\delta \tag{2}$$

and where $N(m,\sigma^2) = m + \sigma N(0,1)$ is a shifted, scaled version of the zero-mean, unit-variance Gaussian random variable $N(0,1)$ that has probability density

$$\phi(x) \triangleq \frac{1}{\sqrt{2\pi}} e^{-x^2/2} \tag{3}$$

The Webb+Gaussian random variable $W(m,\sigma^2,\delta^2) + N(m',\sigma'^2)$ can also be written as a shifted, scaled version of a composite zero-mean, unit-variance random variable, as

$$\begin{aligned} W(m,\sigma^2,\delta^2) + N(m',\sigma'^2) &\triangleq WG(m+m', \sigma^2+\sigma'^2, \delta^2, \beta) \\ &= m + m' + \sqrt{\sigma^2+\sigma'^2}\left(\sqrt{\beta}W(0,1,\delta^2) + \sqrt{1-\beta}N(0,1)\right) \end{aligned}$$

where $\beta = \sigma^2/(\sigma^2+\sigma'^2)$. The term in parentheses is a zero-mean, unit-variance random variable, $WG(0,1,\delta^2,\beta)$, with probability density

$$\phi(x;\delta^2,\beta) = \int_{-\delta}^{\infty} \frac{1}{\sqrt{\beta}}\, \phi\left(\frac{w}{\sqrt{\beta}};\delta^2\right) \frac{1}{\sqrt{1-\beta}}\, \phi\left(\frac{x-w}{\sqrt{1-\beta}}\right) dw \tag{4}$$

B. Capacity

From [1], the capacity of soft-decision M-PPM on the Webb+Gaussian channel in bits per channel use is[4]

$$C = \log_2 M - E_{\mathbf{v}|\mathbf{x_1}} \log_2 \sum_{j=1}^{M} \frac{\phi\left(\sqrt{\frac{\rho_+}{\rho_0+\rho_+}}(v_j - \sqrt{\rho_0}); \frac{\rho_0+\beta_0\rho_+}{\rho_0}\Delta, \frac{\rho_0+\beta_0\rho_+}{\rho_0+\rho_+}\right)\ \phi\left(v_1; \frac{\beta_0\rho_+}{\rho_0}\Delta, \beta_0\right)}{\phi\left(\sqrt{\frac{\rho_+}{\rho_0+\rho_+}}(v_1 - \sqrt{\rho_0}); \frac{\rho_0+\beta_0\rho_+}{\rho_0}\Delta, \frac{\rho_0+\beta_0\rho_+}{\rho_0+\rho_+}\right)\ \phi\left(v_j; \frac{\beta_0\rho_+}{\rho_0}\Delta, \beta_0\right)} \tag{5}$$

[4] The cited article had an error in this expression. The corrected expression is given here.

where the four fundamental parameters are

$$\rho_0 \triangleq \frac{(m_1 - m_0)^2}{\sigma_0^2 + \sigma'^2} \tag{6}$$

$$\rho_+ \triangleq \frac{(m_1 - m_0)^2}{\sigma_1^2 - \sigma_0^2} \tag{7}$$

$$\Delta \triangleq \delta_1^2 - \delta_0^2 \tag{8}$$

$$\beta_0 \triangleq \frac{\sigma_0^2}{\sigma_0^2 + \sigma'^2} \tag{9}$$

and where the components of $\mathbf{v}$ are distributed as

$$v_j \sim \begin{cases} WG\left(\sqrt{\rho_0}, \dfrac{\rho_0 + \rho_+}{\rho_+}, \Delta + \dfrac{\beta_0\rho_+\Delta}{\rho_0}, \dfrac{\rho_0 + \beta_0\rho_+}{\rho_0 + \rho_+}\right) & j = 1 \\ WG\left(0, 1, \dfrac{\beta_0\rho_+\Delta}{\rho_0}, \beta_0\right) & j \neq 1 \end{cases} \tag{10}$$

The capacity can be rewritten as

$$C = \log_2 M - E_{\mathbf{v}|\mathbf{x}_1} \log_2 \left[\sum_{j=1}^{M} \frac{L(v_j)}{L(v_1)}\right] \tag{11}$$

where

$$L(v_j) = \frac{\phi\left(\sqrt{\dfrac{\rho_+}{\rho_0 + \rho_+}}(v_j - \sqrt{\rho_0}); \dfrac{\rho_0 + \beta_0\rho_+}{\rho_0}\Delta, \dfrac{\rho_0 + \beta_0\rho_+}{\rho_0 + \rho_+}\right)}{\phi\left(v_j; \dfrac{\beta_0\rho_+}{\rho_0}\Delta, \beta_0\right)} \tag{12}$$

is the likelihood ratio of v_j.

C. Relationship of Fundamental and Physical Parameters

The capacity of soft-decision M-ary PPM on the Webb+Gaussian channel given by Eq. (11) is a real-valued function $C(\mathbf{a})$, where $\mathbf{a} = (\rho_0, \rho_+, \Delta, \beta_0)$ is the vector of fundamental parameters. The fundamental parameter vector $\mathbf{a}$ can be expressed in terms of physical parameters

$$P = \{\eta, \bar{n}_s, \bar{n}_b, F, I_b, I_s, T_s, T, R_L, G\}$$

by

$$\rho_0 \triangleq \frac{(m_1 - m_0)^2}{\sigma_0^2 + \sigma'^2} = \frac{G^2\eta^2\bar{n}_s^2}{FG^2\left(\eta\bar{n}_b + \dfrac{I_bT_s}{e_-}\right) + \dfrac{I_sT_s}{e_-} + \dfrac{2\kappa TT_s}{R_Le_-^2}} \tag{13}$$

$$\rho_+ \triangleq \frac{(m_1 - m_0)^2}{\sigma_1^2 - \sigma_0^2} = \frac{\eta\bar{n}_s}{F} \tag{14}$$

$$\Delta \triangleq \delta_1^2 - \delta_0^2 = \frac{\eta\bar{n}_sF}{(F-1)^2} \tag{15}$$

$$\beta_0 \triangleq \frac{\sigma_0^2}{\sigma_0^2 + \sigma'^2} = \frac{1}{1 + \dfrac{\sigma'^2}{\sigma_0^2}} = \frac{1}{1 + \dfrac{\dfrac{I_sT_s}{e_-} + \dfrac{2\kappa TT_s}{R_Le_-^2}}{FG^2\left(\eta\bar{n}_b + \dfrac{I_bT_s}{e_-}\right)}} \tag{16}$$

Expressions of parameters m_0, m_1, σ_0^2, σ_1^2, σ'^2, δ_0^2, and δ_1^2 in terms of the physical parameters can be found in, e.g., [1,2,6]. See Appendix A for a review of all the parameters used in this article.

III. Capacity Sensitivity

The sensitivity of capacity to a fundamental or physical parameter x at operating point $\mathbf{a}$ is defined as the partial derivative of the logarithm of capacity with respect to the logarithm of the parameter:

$$\text{capacity sensitivity with respect to } x \triangleq \frac{\partial \log C(\mathbf{a})}{\partial \log x}$$

The logarithm is used to emphasize the sensitivity of the parameter *without regard to the units in which the parameter is measured*, and it allows us to effectively compare the relative sensitivities of various parameters. This is in contrast to the linear partial derivative $\partial C/\partial x$, which has one value when, for example, $x = T_s$ is measured in nanoseconds, and a value one billion times smaller when $x = T_s$ is measured in seconds. If x is a physical parameter, we may express the sensitivity with respect to x at operating point $\mathbf{a}$ as

$$\frac{\partial \log C(\mathbf{a})}{\partial \log x} = \left(\frac{1}{C(\mathbf{a})}\right)\frac{\partial C(\mathbf{a})}{\partial \log x} = \left(\frac{x}{C(\mathbf{a})}\right)\frac{\partial C(\mathbf{a})}{\partial x} \tag{17}$$

$$= \left(\frac{x}{C(\mathbf{a})}\right)\left(\frac{\partial C(\mathbf{a})}{\partial \rho_0}\frac{\partial \rho_0}{\partial x} + \frac{\partial C(\mathbf{a})}{\partial \rho_+}\frac{\partial \rho_+}{\partial x} + \frac{\partial C(\mathbf{a})}{\partial \Delta}\frac{\partial \Delta}{\partial x} + \frac{\partial C(\mathbf{a})}{\partial \beta_0}\frac{\partial \beta_0}{\partial x}\right)$$

$$= \left(\frac{x}{C(\mathbf{a})}\right)\nabla C(\mathbf{a}) \cdot \frac{\partial \mathbf{a}}{\partial x} \tag{18}$$

i.e., the normalized dot product of the gradient of $C(\mathbf{a})$ and the vector $\partial\mathbf{a}/\partial x$ that forms one of the columns of the Jacobian matrix of $\mathbf{a}$:

$J(\mathbf{a})$

$$= \begin{bmatrix} \frac{\partial \rho_0}{\partial \eta} & \frac{\partial \rho_0}{\partial \bar{n}_s} & \frac{\partial \rho_0}{\partial \bar{n}_b} & \frac{\partial \rho_0}{\partial F} & \frac{\partial \rho_0}{\partial I_b} & \frac{\partial \rho_0}{\partial I_s} & \frac{\partial \rho_0}{\partial T_s} & \frac{\partial \rho_0}{\partial T} & \frac{\partial \rho_0}{\partial R_L} & \frac{\partial \rho_0}{\partial G} \\ \frac{\partial \rho_+}{\partial \eta} & \frac{\partial \rho_+}{\partial \bar{n}_s} & \frac{\partial \rho_+}{\partial \bar{n}_b} & \frac{\partial \rho_+}{\partial F} & \frac{\partial \rho_+}{\partial I_b} & \frac{\partial \rho_+}{\partial I_s} & \frac{\partial \rho_+}{\partial T_s} & \frac{\partial \rho_+}{\partial T} & \frac{\partial \rho_+}{\partial R_L} & \frac{\partial \rho_+}{\partial G} \\ \frac{\partial \Delta}{\partial \eta} & \frac{\partial \Delta}{\partial \bar{n}_s} & \frac{\partial \Delta}{\partial \bar{n}_b} & \frac{\partial \Delta}{\partial F} & \frac{\partial \Delta}{\partial I_b} & \frac{\partial \Delta}{\partial I_s} & \frac{\partial \Delta}{\partial T_s} & \frac{\partial \Delta}{\partial T} & \frac{\partial \Delta}{\partial R_L} & \frac{\partial \Delta}{\partial G} \\ \frac{\partial \beta_0}{\partial \eta} & \frac{\partial \beta_0}{\partial \bar{n}_s} & \frac{\partial \beta_0}{\partial \bar{n}_b} & \frac{\partial \beta_0}{\partial F} & \frac{\partial \beta_0}{\partial I_b} & \frac{\partial \beta_0}{\partial I_s} & \frac{\partial \beta_0}{\partial T_s} & \frac{\partial \beta_0}{\partial T} & \frac{\partial \beta_0}{\partial R_L} & \frac{\partial \beta_0}{\partial G} \end{bmatrix}$$

$=$

$$\begin{bmatrix} \frac{\eta e_-^2 G^2 R_L \bar{n}_s^2 \left(\eta \bar{n}_b e_-^2 F G^2 R_L + 2\left(e_- \left(I_s + F G^2 I_b\right) R_L + 2\kappa T\right) T_s\right)}{\left(\eta \bar{n}_b e_-^2 F G^2 R_L + \left(e_- (I_s + F G^2 I_b) R_L + 2\kappa T\right) T_s\right)^2} & \frac{\bar{n}_s}{F} & \frac{F \bar{n}_s}{(F-1)^2} & \frac{\bar{n}_b e_-^2 F G^2 R_L (e_- I_s R_L + 2\kappa T) T_s}{\left(\eta \bar{n}_b e_-^2 F G^2 R_L + \left(e_- (I_s + F G^2 I_b) R_L + 2\kappa T\right) T_s\right)^2} \\ \frac{2\eta^2 e_-^2 G^2 R_L \bar{n}_s}{\eta \bar{n}_b e_-^2 F G^2 R_L + \left(e_- (I_s + F G^2 I_b) R_L + 2\kappa T\right) T_s} & \frac{\eta}{F} & \frac{\eta F}{(F-1)^2} & 0 \\ \frac{-\eta^3 e_-^4 F G^4 R_L^2 \bar{n}_s^2}{\left(\eta \bar{n}_b e_-^2 F G^2 R_L + \left(e_- (I_s + F G^2 I_b) R_L + 2\kappa T\right) T_s\right)^2} & 0 & 0 & \frac{\eta e_-^2 F G^2 R_L (e_- I_s R_L + 2\kappa T) T_s}{\left(\eta \bar{n}_b e_-^2 F G^2 R_L + \left(e_- (I_s + F G^2 I_b) R_L + 2\kappa T\right) T_s\right)^2} \\ \frac{-\eta^2 e_-^3 G^4 R_L^2 \bar{n}_s^2 (\eta \bar{n}_b e_- + I_b T_s)}{\left(\eta \bar{n}_b e_-^2 F G^2 R_L + \left(e_- (I_s + F G^2 I_b) R_L + 2\kappa T\right) T_s\right)^2} & \frac{-\eta \bar{n}_s}{F^2} & \frac{-\eta(1+F)\bar{n}_s}{(F-1)^3} & \frac{e_- G^2 R_L (e_- I_s R_L + 2\kappa T) T_s (\eta \bar{n}_b e_- + I_b T_s)}{\left(\eta \bar{n}_b e_-^2 F G^2 R_L + \left(e_- (I_s + F G^2 I_b) R_L + 2\kappa T\right) T_s\right)^2} \\ \frac{-\eta^2 e_-^3 F G^4 R_L^2 \bar{n}_s^2 T_s}{\left(\eta \bar{n}_b e_-^2 F G^2 R_L + \left(e_- (I_s + F G^2 I_b) R_L + 2\kappa T\right) T_s\right)^2} & 0 & 0 & \frac{e_- F G^2 R_L (e_- I_s R_L + 2\kappa T) T_s^2}{\left(\eta \bar{n}_b e_-^2 F G^2 R_L + \left(e_- (I_s + F G^2 I_b) R_L + 2\kappa T\right) T_s\right)^2} \\ \frac{-\eta^2 e_-^3 G^2 R_L^2 \bar{n}_s^2 T_s}{\left(\eta \bar{n}_b e_-^2 F G^2 R_L + \left(e_- (I_s + F G^2 I_b) R_L + 2\kappa T\right) T_s\right)^2} & 0 & 0 & \frac{-e_-^2 F G^2 R_L^2 T_s (\eta \bar{n}_b e_- + I_b T_s)}{\left(\eta \bar{n}_b e_-^2 F G^2 R_L + \left(e_- (I_s + F G^2 I_b) R_L + 2\kappa T\right) T_s\right)^2} \\ \frac{-\eta^2 e_-^2 G^2 R_L \bar{n}_s^2 \left(e_- \left(I_s + F G^2 I_b\right) R_L + 2\kappa T\right)}{\left(\eta \bar{n}_b e_-^2 F G^2 R_L + \left(e_- (I_s + F G^2 I_b) R_L + 2\kappa T\right) T_s\right)^2} & 0 & 0 & \frac{-\eta \bar{n}_b e_-^2 F G^2 R_L (e_- I_s R_L + 2\kappa T)}{\left(\eta \bar{n}_b e_-^2 F G^2 R_L + \left(e_- (I_s + F G^2 I_b) R_L + 2\kappa T\right) T_s\right)^2} \\ \frac{-2\eta^2 e_-^2 G^2 k R_L \bar{n}_s^2 T_s}{\left(\eta \bar{n}_b e_-^2 F G^2 R_L + \left(e_- (I_s + F G^2 I_b) R_L + 2\kappa T\right) T_s\right)^2} & 0 & 0 & \frac{-2 e_- F G^2 \kappa R_L T_s (\eta \bar{n}_b e_- + I_b T_s)}{\left(\eta \bar{n}_b e_-^2 F G^2 R_L + \left(e_- (I_s + F G^2 I_b) R_L + 2\kappa T\right) T_s\right)^2} \\ \frac{2\eta^2 e_-^2 G^2 \kappa \bar{n}_s^2 T T_s}{\left(\eta \bar{n}_b e_-^2 F G^2 R_L + \left(e_- (I_s + F G^2 I_b) R_L + 2\kappa T\right) T_s\right)^2} & 0 & 0 & \frac{2 e_- F G^2 \kappa T T_s (\eta \bar{n}_b e_- + I_b T_s)}{\left(\eta \bar{n}_b e_-^2 F G^2 R_L + \left(e_- (I_s + F G^2 I_b) R_L + 2\kappa T\right) T_s\right)^2} \\ \frac{2\eta^2 e_-^2 G R_L \bar{n}_s^2 (e_- I_s R_L + 2\kappa T) T_s}{\left(\eta \bar{n}_b e_-^2 F G^2 R_L + \left(e_- (I_s + F G^2 I_b) R_L + 2\kappa T\right) T_s\right)^2} & 0 & 0 & \frac{2 e_- F G R_L (e_- I_s R_L + 2\kappa T) T_s (\eta \bar{n}_b e_- + I_b T_s)}{\left(\eta \bar{n}_b e_-^2 F G^2 R_L + \left(e_- (I_s + F G^2 I_b) R_L + 2\kappa T\right) T_s\right)^2} \end{bmatrix}^T$$

(Note that the expanded matrix has been written as a transpose.) To determine the sensitivity of capacity with respect to one of the physical parameters, we need only determine the gradient of the capacity expressed as a function of the four fundamental parameters and form the inner product with the appropriate column of $J(\mathbf{a})$.

IV. Numerical Results

A. Approach

To evaluate the capacity for a given set of fundamental parameters, ρ_0, ρ_+, Δ, and β_0, we generate a random vector $\mathbf{v} = (v_1, \cdots, v_M)$ according to Eq. (10), evaluate the logarithmic function in Eq. (11), and average the computed logarithm over several million such random vector samples. In order to avoid performing the hundreds of millions of resulting convolution integrals, we save a look-up table for the likelihood ratio $L(v)$ over a wide range of v. The range needs to be chosen large enough so that millions of random samples drawn from either probability density function (pdf) in Eq. (10) are unlikely to take on values outside of this range. This is accomplished with a range from eight standard deviations below the mean of $v_j, j \geq 2$ to eight standard deviations above the mean of v_1. To obtain sufficient resolution, a uniformly quantized table of size 10,000 is used within this range, which requires computation of 20,000 convolution integrals. The table requires approximately 15 seconds of computation time on a Pentium-II 333 and saves over 1,000 hours of computation time if the overall simulation uses 10 million sample vectors. A typical likelihood ratio $L(v)$ over the range stored in the look-up table is shown in Fig. 1.

The gradient of the capacity is computed by finite differences: the capacity is determined at a nominal operating point, $\mathbf{a}_0 = (\rho_0, \rho_+, \Delta, \beta_0)$, and then at the operating points

$$\mathbf{a}_1 = (\rho_0 - \epsilon, \rho_+, \Delta, \beta_0)$$

$$\mathbf{a}_2 = (\rho_0, \rho_+ - \epsilon, \Delta, \beta_0)$$

$$\mathbf{a}_3 = (\rho_0, \rho_+, \Delta - \epsilon, \beta_0)$$

$$\mathbf{a}_4 = (\rho_0, \rho_+, \Delta, \beta_0 - \epsilon)$$

Each of the operating points requires its own look-up table for $L(v)$. The gradient is then given by

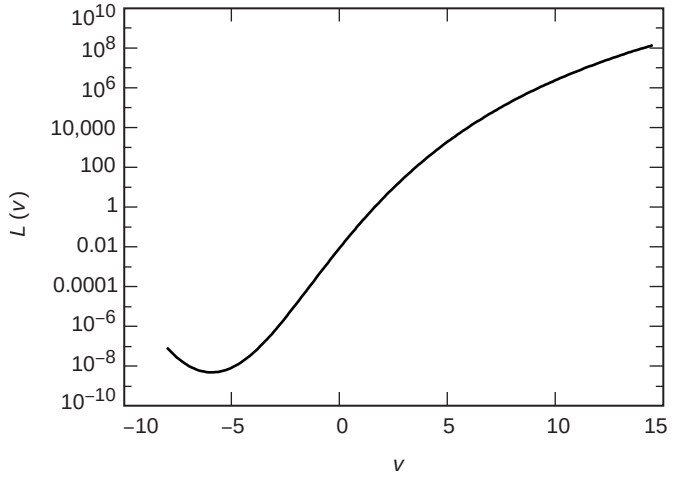

Fig. 1. Likelihood ratio *L* (*v*) over the range stored in the look-up table, Case 1.

$$\nabla C(\mathbf{a}_0) \approx \left(\frac{C(\mathbf{a}_0) - C(\mathbf{a}_1)}{\epsilon}, \frac{C(\mathbf{a}_0) - C(\mathbf{a}_2)}{\epsilon}, \frac{C(\mathbf{a}_0) - C(\mathbf{a}_3)}{\epsilon}, \frac{C(\mathbf{a}_0) - C(\mathbf{a}_4)}{\epsilon} \right)$$

Following the calculation of the gradient, the inner product is formed with the appropriate column of $J(\mathbf{a})$.

B. Results at Specific Operating Points

1. Case 1: Strong Signal, Strong Background, Optimized Gain. Here we consider a PerkinElmer SliK APD detector with physical parameters $\eta = 0.38$, $F = 2.42572$, $I_b = 40$ fA, $I_s = 2.00$ nA, $T = 300$ K, and $R_L = 179.7$ kΩ. It has been shown [3,5] that, for this set of parameters, $G = 65$ is the optimum gain for hard-decision detection of 256-PPM. This is also a good estimate of the gain that maximizes capacity on the soft-decision channel, which turned out to be $G = 59$. We use a Q-switched Nd:YAG laser modulated with a slot width of $T_s = 31.25$ ns. A high signal strength, $\bar{n}_s = 100$, is incident on the detector, and a high background level, $\bar{n}_b = 100$, is also present, which corresponds to reception on a clear, sunny day.

Plugging these parameters into Eqs. (13) through (16), it follows that $\rho_0 = 13.7$, $\rho_+ = 15.7$, $\Delta = 45.3$, and $\beta_0 = 0.873$. The likelihood ratio $L(v)$ computed for these parameters is shown in Fig. 1. Using the finite differences method described above, the partial derivative of capacity with respect to each fundamental parameter, i.e., the components of the gradient, was computed. These components, when normalized as in Eq. (17), give the capacity sensitivity with respect to each of the fundamental parameters, which is shown in Fig. 2. Note that by far the SNR parameter, ρ_0, has the greatest effect on capacity, followed by the excess SNR parameter, ρ_+. The blending fraction, β_0, and skewness difference, Δ, play lesser roles.

The Jacobian matrix was evaluated (see numerical value in Appendix B) and used to determine the $\partial C/\partial x$ for each physical parameter x. The capacity sensitivity with respect to the physical parameters is shown in Fig. 3.

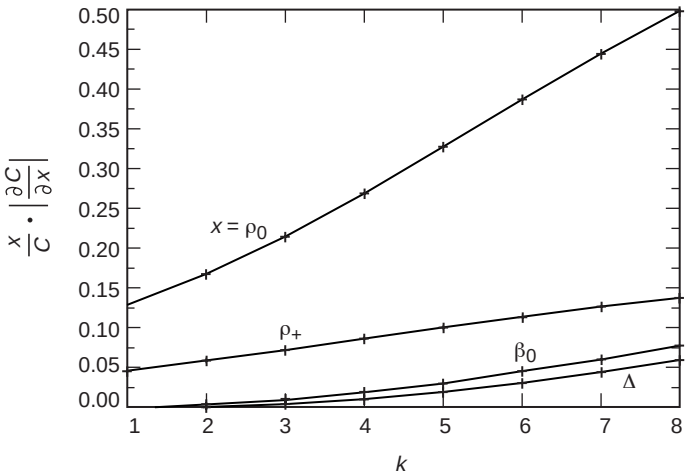

Fig. 2. Capacity sensitivity of 2^K-PPM, with respect to fundamental parameters, Case 1.

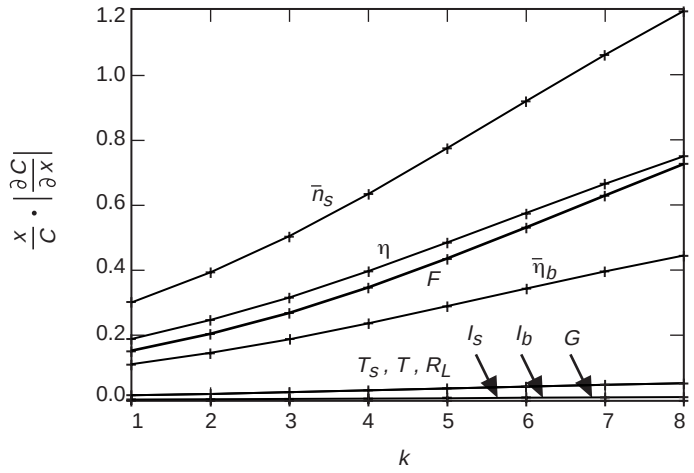

Fig. 3. Capacity sensitivity of 2^k-PPM, with respect to physical parameters, Case 1.

As is no surprise, the signal intensity, $\bar{n}_s$, and background intensity, $\bar{n}_b$, are two of the most important physical parameters. Curiously, capacity sensitivity with respect to $\bar{n}_s$ is approximately twice the sensitivity with respect to $\bar{n}_b$. This contrasts with the usual AWGN channel, where signal and noise affect capacity in precisely equal amounts, i.e., only through their ratio. Also, note that sensitivity of $\bar{n}_s$ is the sum of the sensitivities of $\bar{n}_b$ and η. This is a consequence of the fact that the number of absorbed photons is proportional to η.

The most capacity-sensitive detector parameter is the quantum efficiency, η, which at the operating point shown is even more influential than the background intensity. Capacity is also sensitive to the excess noise ratio, F. The slot width, T_s; noise temperature, T; and load resistance, R_L, play lesser roles, and are nearly equal because of their occurrence together in Eqs. (13) and (16). Capacity sensitivity with respect to both I_b and I_s is more than two orders of magnitude lower than the other parameters. This is because I_s and I_b contribute only negligibly to ρ_0 and β_0 at this operating point as compared with the other physical parameters in Eqs. (13) and (16). Since the gain has been optimized, capacity is not sensitive to the gain.

2. Case 2: Strong Signal, Strong Background, Nonoptimized Gain. If we now let $G = 30$ instead of the optimized $G = 59$ used above, we obtain $\rho_0 = 9.95$, $\rho_+ = 17.6$, $\Delta = 60.8$, and $\beta_0 = 0.566$. A full simulation was run to determine $C(\mathbf{a})$ and $\nabla C(\mathbf{a})$ at this operating point. The capacity sensitivities with respect to the fundamental parameters are shown in Fig. 4. Again, the SNR parameter, ρ_0, has by far the greatest effect on capacity, followed by the excess SNR parameter, ρ_+. And again, the blending fraction, β_0, and skewness difference, Δ, play lesser roles.

The Jacobian matrix for Case 2 is given in Appendix B, from which we obtain the capacity with respect to the physical parameters. The capacity sensitivity with respect to the physical parameters is shown in Fig. 5. As can be seen, capacity is sensitive in a very similar way to that in Case 1, except that the non-optimized gain, G, is easily identified by its much larger value. In this case, the capacity sensitivity with respect to G is about ten times that in Case 1, which is an indication that capacity may be increased by properly increasing the gain.

3. Case 3: Weak Signal, Strong Background. In this weak signal, strong background case, we let $\bar{n}_s = 10$, $\bar{n}_b = 100$, and $G = 30$. Here, $\rho_0 = 0.0995$, $\rho_+ = 1.76$, $\Delta = 6.08$, and $\beta_0 = 0.566$, and the Jacobian matrix is given in Appendix B. A full simulation was run at this operating point. The capacity sensitivities with respect to the fundamental parameters are shown in Fig. 6. Here, the SNR, ρ_0, plays the only non-negligible role, with ρ_+, Δ, and β_0 more than two orders of magnitude behind. This implies

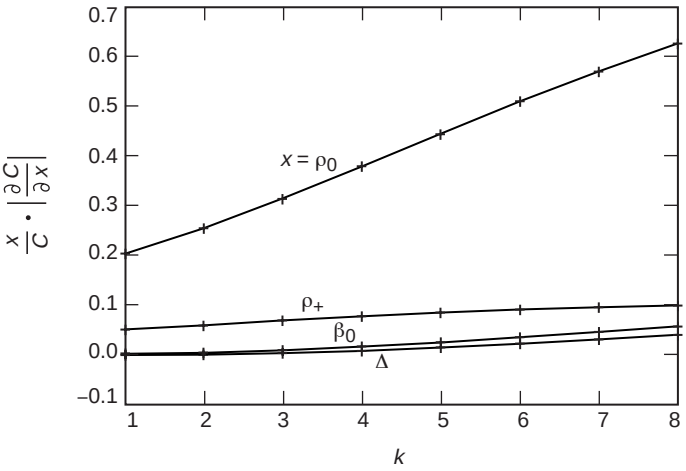

Fig. 4. Capacity sensitivity of 2^k-PPM, with respect to fundamental parameters, Case 2.

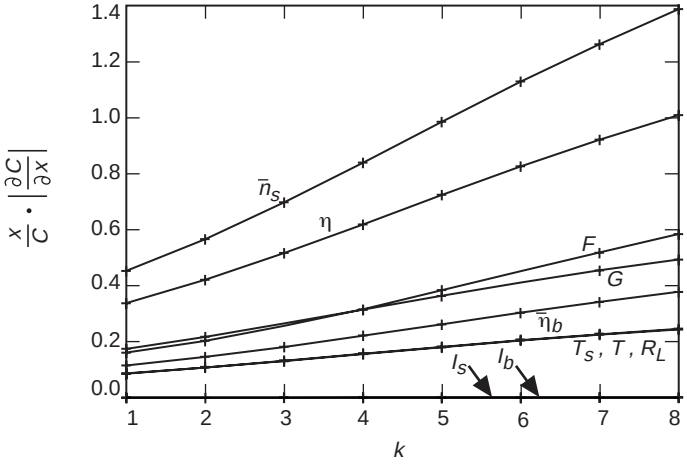

Fig. 5. Capacity sensitivity of 2^k-PPM, with respect to physical parameters, Case 2.

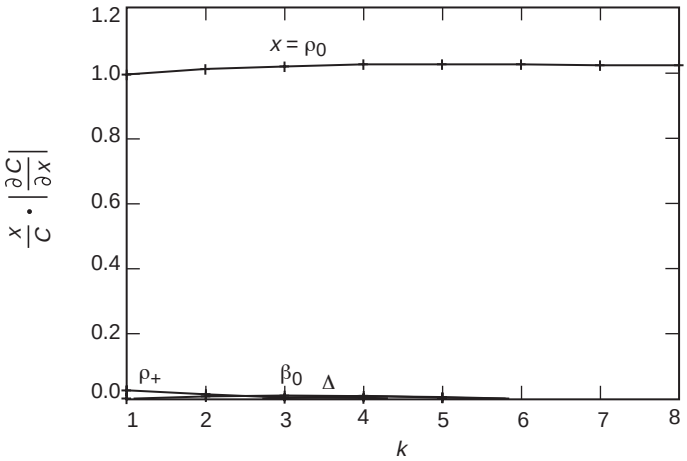

Fig. 6. Capacity sensitivity of 2^k-PPM, with respect to fundamental parameters, Case 3.

that, when the signal strength is low, capacity is almost completely a function of one SNR parameter and is very sensitive to the precise signal level.

Indeed, we see in Fig. 7 that $(\bar{n}_s/C)|\partial C/\partial \bar{n}_s|$ and $(\eta/C)|\partial C/\partial \eta|$ are much higher than in Cases 1 and 2. In fact, they are greater than one, meaning a more than one-for-one return on investment is possible. Capacity sensitivities with respect to other physical parameters are similar to Cases 1 and 2.

4. Case 4: Weak Signal, Weak Background. In Case 4, we let $\bar{n}_s = 10$, $\bar{n}_b = 1$, and $G = 140$. It follows that $\rho_0 = 3.58$, $\rho_+ = 1.28$, $\Delta = 2.93$, $\beta_0 = 0.284$, and the Jacobian matrix is given in Appendix B.

A full simulation was run at this operating point. The capacity sensitivities with respect to the fundamental parameters are shown in Fig. 8. As in all previous cases, the SNR parameter, ρ_0, has the greatest effect on capacity. In this case, however, the skewness difference, Δ, has a greater effect at higher PPM orders than the excess SNR, ρ_+. The sensitivities with respect to both Δ and ρ_+ are significantly higher than in the previous cases, because when both signal and background are weak, the difference of the variances or skewnesses in the signal and nonsignal slots becomes relatively more important in distinguishing signals. As in all previous cases, the fraction of the signal that is Webb distributed, β_0, plays a minor role at this operating point.

The capacity sensitivities with respect to the physical parameters are shown in Fig. 9. As in Case 3, $\bar{n}_s$ and η are the critical physical parameters. The background intensity, $\bar{n}_b$, is even less influential than in Cases 1 through 3. Reducing the background intensity incident on the detector would not be even as effective as, e.g., reducing the effective noise temperature of the detector.

V. Conclusions

The capacity of the Webb+Gaussian channel was derived analytically and evaluated numerically in four cases. In conjunction with a Jacobian matrix that describes the relationship between four fundamental parameters and ten physical parameters, this allowed us to determine the sensitivity of the capacity with respect to any of the four fundamental parameters and any single physical parameter.

In all cases considered, the capacity was found to be most sensitive to the primary SNR parameter, ρ_0, with the other three fundamental parameters playing lesser roles.

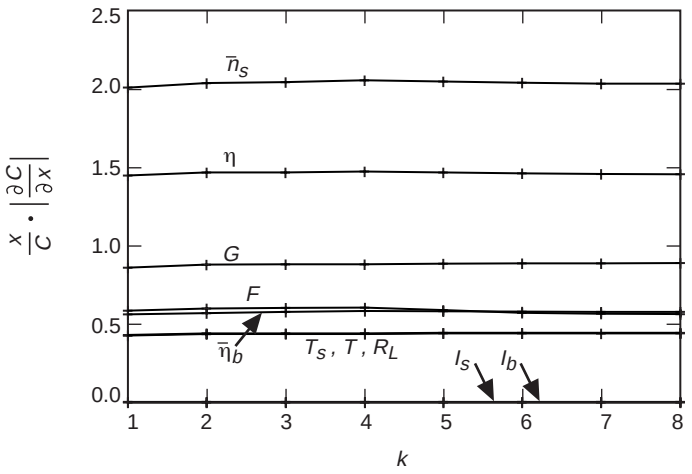

Fig. 7. Capacity sensitivity of 2^k-PPM, with respect to physical parameters, Case 3.

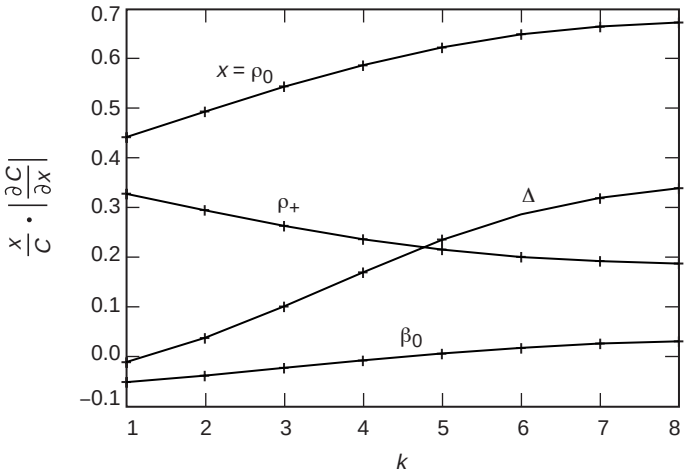

Fig. 8. Capacity sensitivity of 2^k-PPM, with respect to fundamental parameters, Case 4.

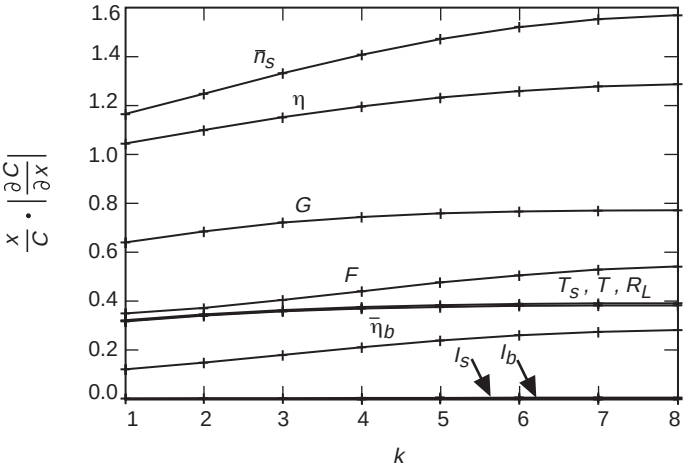

Fig. 9. Capacity sensitivity of 2^k-PPM, with respect to physical parameters, Case 4.

Perhaps the most surprising result is that, in all cases evaluated, the signal intensity has a substantially larger influence on capacity than the background intensity, usually by a factor of two or more. This is particularly true during night reception, in which a 1 percent reduction in background intensity would not increase the capacity as much as, for example, a 1 percent reduction in the equivalent noise temperature or a 1 percent reduction in the excess noise factor of the detector.

There are a number of expected results, as well. The quantum efficiency was shown to be the critical detector parameter and was found to be more influential than any other physical parameter except the signal intensity. When the gain was not optimized, the capacity was sensitive to small gain fluctuations; when the gain was optimized, the capacity was not sensitive to small gain fluctuations. The leakage currents affected capacity much less than the other parameters, by multiple orders of magnitude.

The overall relative importance of the physical parameters, with respect to capacity sensitivity, was found to be fairly consistent. The physical parameters, in order of influence, are the signal intensity, the quantum efficiency, the excess noise factor, the background intensity, the gain, the slot width, the equivalent noise temperature, the load resistance, the surface leakage current, and the bulk leakage current.

References

[1] S. Dolinar, D. Divsalar, J. Hamkins, and F. Pollara, "Capacity of Pulse-Position Modulation (PPM) on Gaussian and Webb Channels," *The Telecommunications and Mission Operations Progress Report 42-142, April–June 2000*, Jet Propulsion Laboratory, Pasadena, California, pp. 1–31, August 15, 2000.
http://tmo.jpl.nasa.gov/tmo/progress_report/42-142/142H.pdf

[2] F. M. Davidson and X. Sun, "Gaussian Approximation Versus Nearly Exact Performance Analysis of Optical Communication Systems with PPM Signaling and APD Receivers," *IEEE Trans. Commun.*, vol. 36, no. 11, pp. 1185–1192, November 1988.

[3] J. Hamkins, "The Capacity of Avalanche Photodiode-Detected Pulse-Position Modulation," *The Telecommunications and Mission Operations Progress Report 42-138, April–June 1999*, Jet Propulsion Laboratory, Pasadena, California, pp. 1–19, August 15, 1999.
http://tmo.jpl.nasa.gov/tmo/progress_report/42-138/138A.pdf

[4] G. S. Mecherle, *Maximized Data Rate Capability for Optical Communication Using Semiconductor Devices with Pulse Position Modulation*, Ph.D. thesis, University of Southern California, Los Angeles, May 1986.

[5] M. Srinivasan and V. Vilnrotter, "Symbol-Error Probabilities for Pulse-Position Modulation Signaling With an Avalanche Photodiode Receiver and Gaussian Thermal Noise," *The Telecommunications and Mission Operations Progress Report 42-134, April–June 1998*, Jet Propulsion Laboratory, Pasadena, California, pp. 1–11, August 15, 1998.
http://tmo.jpl.nasa.gov/tmo/progress_report/42-134/134E.pdf

[6] J. T. K. Tang and K. B. Letaief, "The Use of WMC Distribution for Performance Evaluation of APD Optical Communication Systems," *IEEE Trans. Commun.*, vol. 46, no. 2, pp. 279–285, February 1998.

Appendix A
Parameters

	Fundamental parameters	
ρ_0	$\triangleq \frac{(m_1 - m_0)^2}{\sigma_0^2 + \sigma'^2}$	Slot SNR
ρ_+	$\triangleq \frac{(m_1 - m_0)^2}{\sigma_1^2 - \sigma_0^2}$	Excess slot SNR
Δ	$\triangleq \delta_1^2 - \delta_0^2$	Difference of Webb skewness in signaling and nonsignaling slots
β_0	$\triangleq \frac{\sigma_0^2}{\sigma_0^2 + \sigma'^2}$	Fraction of APD output having Webb distribution
	Channel description parameters	
m_0, m_1		Mean of Webb component of nonsignaling, signaling slot statistic
σ_0^2, σ_1^2		Variance of Webb component of nonsignaling, signaling slot statistic
m'		Mean of AWGN component of slot statistic
σ'^2		Variance of AWGN component of slot statistic
δ_0^2, δ_1^2		Skewness of Webb component of nonsignaling, signaling slot statistic
	Laser and modulator parameters	
M	2–256	PPM order
T_s	3.125×10^{-8}	Width of the PPM slot required by laser, s
	APD detector parameters	
η	38%	Quantum efficiency
F	2.2–3.4	Excess noise factor, $F = k_{eff}G + \left(\frac{2-1}{G}\right)(1 - k_{eff})$
I_b	4×10^{-14}	Bulk leakage current, A
I_s	2×10^{-9}	Surface leakage current, A
T	300	Noise temperature, K
R_L	179,700	Load resistance (transimpedance model), $5.75 \times 10^{12} \times T_s$, Ω
B	$\frac{1}{2T_s}$	Noise equivalent one-sided bandwidth, Hz
G	30–200	Gain
	Other parameters	
$\bar{n}_b$	0.001–10,000	Mean background photons incident on the photodetector, per slot
$\bar{n}_s$	100	Mean signal photons incident on the photodetector, per pulse
	Physical constants	
κ	1.38×10^{-23}	Boltzmann's constant, J/K
e_-	1.6×10^{-19}	Electron charge, C

Appendix B
Numerical Evaluation of $J(\mathbf{a})$

The numerical values of the Jacobian matrices for Cases 1 through 4 are given below.

I. Case 1

$$J(\mathbf{a}) = \begin{bmatrix} 40.6 & 0.273 & -0.119 & -4.92 & -6.13 \times 10^{10} \\ 41.2 & 0.157 & 0 & -6.46 & 0 \\ 119 & 0.453 & 0 & -44.9 & 0 \\ -0.292 & 0 & -0.00111 & -0.0457 & -5.7 \times 10^{8} \end{bmatrix} \cdots$$

$$\cdots \begin{bmatrix} -5.99 \times 10^{6} & -5.56 \times 10^{7} & -0.00575 & 9.59 \times 10^{-6} & 0.0534 \\ 0 & 0 & 0 & 0 & 0 \\ 0 & 0 & 0 & 0 & 0 \\ 3.82 \times 10^{5} & 3.55 \times 10^{6} & 0.000367 & -6.12 \times 10^{-7} & -0.00341 \end{bmatrix}$$

II. Case 2

$$J(\mathbf{a}) = \begin{bmatrix} 37.5 & 0.199 & -0.0563 & -2.61 & -2.9 \times 10^{10} \\ 46.2 & 0.176 & 0 & -8.12 & 0 \\ 160 & 0.608 & 0 & -76.4 & 0 \\ -0.646 & 0 & -0.00246 & -0.114 & -1.26 \times 10^{9} \end{bmatrix} \cdots$$

$$\cdots \begin{bmatrix} -1.49 \times 10^{7} & -1.38 \times 10^{8} & -0.0143 & 2.38 \times 10^{-5} & 0.288 \\ 0 & 0 & 0 & 0 & 0 \\ 0 & 0 & 0 & 0 & 0 \\ 8.47 \times 10^{5} & 7.86 \times 10^{6} & 0.000813 & -1.36 \times 10^{-6} & -0.0164 \end{bmatrix}$$

III. Case 3

$$J(\mathbf{a}) = \begin{bmatrix} 0.375 & 0.0199 & -0.000563 & -0.0261 & -2.9 \times 10^{8} \\ 4.62 & 0.176 & 0 & -0.812 & 0 \\ 16 & 0.608 & 0 & -7.64 & 0 \\ -0.646 & 0 & -0.00246 & -0.114 & -1.26 \times 10^{9} \end{bmatrix} \cdots$$

$$\cdots \begin{bmatrix} -1.49 \times 10^{5} & -1.38 \times 10^{6} & -0.000143 & 2.38 \times 10^{-7} & 0.00288 \\ 0 & 0 & 0 & 0 & 0 \\ 0 & 0 & 0 & 0 & 0 \\ 8.47 \times 10^{5} & 7.86 \times 10^{6} & 0.000813 & -1.36 \times 10^{-6} & -0.0164 \end{bmatrix}$$

IV. Case 4

$$J(\mathbf{a}) = \begin{bmatrix} 16.2 & 0.715 & -0.996 & -0.344 & -5.12 \times 10^{11} & \cdots \\ 3.38 & 0.128 & 0 & -0.434 & 0 & \\ 7.71 & 0.293 & 0 & -2 & 0 & \\ -0.525 & 0 & -0.199 & -0.0688 & -1.02 \times 10^{11} & \end{bmatrix}$$

$$\begin{matrix} & -8.83 \times 10^{6} & -8.26 \times 10^{7} & -0.00847 & 1.41 \times 10^{-5} & 0.0366 \\ \cdots & 0 & 0 & 0 & 0 & 0 \\ & 0 & 0 & 0 & 0 & 0 \\ & 7.02 \times 10^{5} & 6.38 \times 10^{6} & 0.000673 & -1.12 \times 10^{-6} & -0.00291 \end{matrix} \Bigg]$$